International Journal of Multidisciplinary Research and Publications
ISSN (Online): 2581-6187

Theoretical Investigation of Quantum Confinement Effects on Bandgap Changes in MoS_2 for Photocatalytic Water Splitting

Moses G. Udoisoh
Department of Physics, Ignatius Ajuru Unversity of Education, Rumuolumini, Port-Harcourt, Nigeria
Email: moses.udoisoh@iaue.edu.ng

Abstract— *The increasing demand for sustainable energy solutions has prompted the exploration of hydrogen fuel production through photocatalytic water splitting, where efficient photocatalysts are crucial. Molybdenum disulfide (MoS_2) has been identified as a promising material due to its bandgap energy range of 1.8-2.1 eV. However, its efficiency is limited by low quantum efficiency and rapid charge recombination. To address these limitations, this study investigates the impact of quantum confinement on MoS_2's bandgap energy using a particle-in-a-box model with soft wall boundary conditions and the time-independent Schrödinger equation. Our results reveal that reducing confinement dimensions significantly increases the bandgap energy. Specifically, the optimal bandgap energy for photocatalytic water splitting ($1.23 - 2.2\ eV$) is achieved at a confinement dimension of approximately $2nm$, yielding a bandgap energy of 2.134 eV. This quantitative analysis highlights the profound influence of nanoconfinement on MoS_2's electronic properties and provides crucial insights for designing efficient photocatalysts. Our findings offer a viable pathway to enhance the photocatalytic activity of MoS_2, supporting the development of sustainable hydrogen fuel production technologies. This research contributes to global efforts to tackle critical energy and environmental challenges, emphasizing the significance of nanoconfinement effects in advancing renewable energy solutions.*

Keywords— *Bandgap energy, Hydrogen fuel production, Molybdenum disulfide (MoS_2), Photocatalysts, Quantum confinement*

I. INTRODUCTION

The challenge of meeting increasing energy demands while addressing climate change has led to a focus on hydrogen fuel as a promising solution (Srinivasadesikan et al., 2022). Water splitting for hydrogen production requires efficient photocatalysts, with the bandgap energy being a crucial factor in determining the efficiency of the process (Yuan et al., 2021). Molybdenum disulfide (MoS_2) has emerged as a potential photocatalyst due to its suitable bandgap energy range of 1.8-2.1 eV (Nawz et al., 2020). However, MoS_2 faces limitations such as low quantum efficiency and fast charge recombination, impacting its overall efficiency (Almansoori, 2023).

Nanoconfinement has emerged as a promising strategy to enhance the photocatalytic performance of materials like molybdenum disulfide (MoS_2) by adjusting their bandgap (Chang et al., 2014). MoS_2, known for its suitable bandgap and high catalytic activity, faces limitations in light absorption within the visible spectrum due to its intrinsic bandgap ((Lin et al., 2022; Yin et al., 2014). By confining MoS_2 at the nanoscale, its electronic structure and properties can be significantly altered, potentially shifting its bandgap and improving its efficiency as a photocatalyst (Wang et al., 2018; Gough et al., 2017; Abe et al., 2005).

Research has shown that nanoconfinement can influence the electronic properties of MoS_2 (Zhang et al., 2019), with composites like MoS_2/CdS demonstrating enhanced activity for photocatalytic water splitting (Zhang et al., 2019). However, a comprehensive theoretical examination focusing on how nanoconfinement affects the bandgap of MoS_2 for enhanced photocatalytic activity is still lacking (Cheng, 2023; Rouzhahong et al., 2020). To address this gap, this study develops a particle-in-a-box model with soft wall boundary conditions using the time-independent Schrödinger equation to explore the impact of quantum confinement on MoS_2's bandgap energy (Gusarov, 2024). The particle in the box model is well-suited for examining nanoconfinement effects on MoS_2 because it allows for the incorporation of material-specific properties and confinement dimensions (Sun, 2023; Новоселов et al., 2016; Kang et al., 2014). Through a first principles approach, the research aims to provide a comprehensive understanding of how quantum confinement influences MoS_2's bandgap energy and, by extension, its photocatalytic capabilities (Ito et al., 2019; Cui et al., 2018; Wang et al., 2017).

This investigation is significant as it addresses a critical gap in knowledge regarding MoS_2's electronic properties and their implications for water splitting efficiency (Aggarwal et al., 2020). The outcomes of this study are expected to contribute valuable insights for the design and development of efficient photocatalysts, thereby supporting global efforts to tackle energy and environmental challenges (Aggarwal et al., 2021).

II. METHODS

To explore the nanoconfinement effects on the bandgap changes in MoS_2, we utilized a particle-in-a-box model incorporating soft wall boundary conditions. This model choice is predicated on its effectiveness in simulating quantum confinement effects, which are pivotal in altering electronic properties due to dimensional constraints. The governing equation of our model is the time-independent Schrödinger equation:

$$-\hbar\nabla\psi(x,y) + V(x,y)\psi(x,y) = E\psi(x,y) \qquad (1)$$

where $\psi(x,y)$ is the wave function, $V(x,y)$ is the confinement potential, and E is the energy eigenvalue.

Moses G. Udoisoh, "Theoretical Investigation of Quantum Confinement Effects on Bandgap Changes in MoS_2 for Photocatalytic Water Splitting," *International Journal of Multidisciplinary Research and Publications (IJMRAP)*, Volume 7, Issue 2, pp. 132-136, 2024.

Confinement Potential

The confinement potential, $V(x,y)$ is crucial in simulating the effects of nanoconfinement. For our model, the potential is expressed as:

$$V(x,y) = V_0\left[1 - cos\left(\frac{\pi x}{L_x}\right)\right]\left[1 - cos\left(\frac{\pi y}{L_y}\right)\right] \quad (2)$$

Here, V_0 is the potential height, and L_x and L_y are the confinement dimensions along the x and y axes, respectively.
Assuming a separable solution of the form:

$$\psi(x,y) = \psi x(x)\psi y(y)$$

we obtain simplified one-dimensional equations for each spatial dimension:

$$-\hbar\frac{\partial\psi_x(x)}{\partial x} + V(x)\psi_x(x) = E_x\psi_x(x) (3)$$

$$-\hbar\frac{\partial\psi_y(y)}{\partial y} + V(y)\psi_y(y) = E_y\psi_y(y) (4)$$

where E_x and E_y are the energy components associated with the x and y dimensions.
Solving (3) and (4), we derive the energy eigenvalues for each state:

$$E(n,m) = \left(\frac{\hbar^2\pi^2}{2m}\right)\left[\left(\frac{n^2}{L_x^2}\right) + \left(\frac{m^2}{L_y^2}\right)\right] (5)$$

where n and m are quantum numbers corresponding to the quantization in the x and y dimensions.

The corresponding normalized wave functions for each dimension are given by:

$$\psi_x(x) = \sqrt{\frac{2}{L_x}}\, sin\left(\frac{n\pi x}{L_x}\right) (6)$$

$$\psi_y(y) = \sqrt{\frac{2}{L_y}}\, sin\left(\frac{m\pi y}{L_y}\right) (7)$$

Determination of Quantum Numbers

We determine the quantum numbers (n, m) for the Valence Band Maximum E_V by considering MoS_2's electronic configuration and the Pauli Exclusion Principle, assuming two electrons per quantum state. The highest occupied state's quantum numbers are selected to accommodate all valence electrons.
The Valence Band Maximum E_v is obtained from (5) as;

$$E_v = \left(\frac{\hbar^2\pi^2}{2m_h}\right)\left[\left(\frac{n^2}{L_x^2}\right) + \left(\frac{m^2}{L_y^2}\right)\right] (8)$$

m_h is the effective mass of holes, different from the electron mass due to material properties.

Conduction Band Minimum (E_C)

The first unoccupied state's quantum numbers are either $n+1$ or $m+1$, depending on the direction (x *or* y) with lower energy, influenced by confinement dimensions L_x and L_y, and electron effective mass.

The Conduction Band Minimum (E_C) is obtained from (5) as;

$$E_c = \left(\frac{\hbar^2\pi^2}{2m_e}\right)\left[\left(\frac{n^2}{L_x^2}\right) + \left(\frac{m^2}{L_y^2}\right)\right] (9)$$

Bandgap Energy Calculation

The bandgap energy E_g is calculated as the difference between the conduction band minimum energy E_c and the valence band maximum energy E_v:

$$E_{g,nano} = E_c - E_v (10)$$

The nanoconfinement-induced bandgap changes ΔE_g is calculated as the difference between the nanoconfined and bulk bandgap energies:

$$\Delta E_g = E_{g,nano} - E_{g,bulk} (11)$$

For photocatalytic applications, we assume confinement similar to monolayer MoS_2, $E_{g,bulk} = 1.8$ eV

III. RESULTS

Equation (8) was used to compute the Valence Band Maximum E_v. The Conduction Band Minimum (E_C)

Was computed with (9). The nano bandgap energy bandgap energy $E_{g,nano}$ and nanoconfinement-induced bandgap changes ΔE_g were calculated with (10) and (11) respectively using the constants;

1. Reduced Planck's Constant $\hbar = 1.0545718 \times 10^{-34} Js$
2. Effective Mass of Electron $m_e = 0.5 \times 9.11 \times 10^{-31} kg$
3. Effective Mass of Holes $m_h = 0.6 \times 9.11 \times 10^{-31} kg$
4. Bulk Bandgap Energy for MoS_2 ($E_g\ bulk$): 1.8 eV
5. Conversion Factor from Joules to Electron Volts: $1eV = 1.6 \times 10^{-19} J$
6. Quantum Number (n):
   a. Valence band: $n = 2$
   b. Conduction band: $n = 3$

Table 1 shows the calculated nano bandgap energies $E_{g,nano}$ for MoS_2 under various confinement dimensions L_x and L_y. The energies are in electron volts (eV) and illustrate the impact of quantum confinement on the bandgap energy, which is crucial for optimizing photocatalytic water splitting.

TABLE 1: Nano Bandgap Energies $E_{g,nano}$(eV)

L_x\L_y (nm)	**1**	**2**	**3**	**4**	**5**
1	5.02	3.14	2.79	2.67	2.61
2	3.14	1.26	0.91	0.78	0.73
3	2.79	0.91	0.56	0.44	0.38
4	2.67	0.78	0.44	0.31	0.26
5	2.61	0.73	0.38	0.26	0.20
6	2.58	0.70	0.35	0.23	0.17
7	2.56	0.68	0.33	0.21	0.15
8	2.55	0.67	0.32	0.20	0.14
9	2.54	0.66	0.31	0.19	0.13
10	2.54	0.65	0.30	0.18	0.13

Table 1 presents the nano bandgap energies $E_{g,nano}$ for MoS_2 as a function of varying confinement dimensions L_x and L_y, both ranging from 1 nm to 10 nm. The data illustrates the quantum confinement effects on the bandgap energy, which is critical for determining the material's suitability for photocatalytic water splitting.

The results show a clear trend where the bandgap energy increases as the confinement dimensions decrease. For instance,

Moses G. Udoisoh, "Theoretical Investigation of Quantum Confinement Effects on Bandgap Changes in MoS_2 for Photocatalytic Water Splitting," *International Journal of Multidisciplinary Research and Publications (IJMRAP)*, Volume 7, Issue 2, pp. 132-136, 2024.

when both L_x and L_y are at their minimum (1 nm), the bandgap energy reaches a maximum value of $5.02eV$. Conversely, as the confinement dimensions increase to $10\,nm$, the bandgap energy significantly decreases, approaching values as low as $0.05\ eV$.

The graph presented in Figure 1 further elucidates the relationship between the nano bandgap energies $E_{g,nano}$ and the varying confinement dimensions L_x for different fixed values of L_y

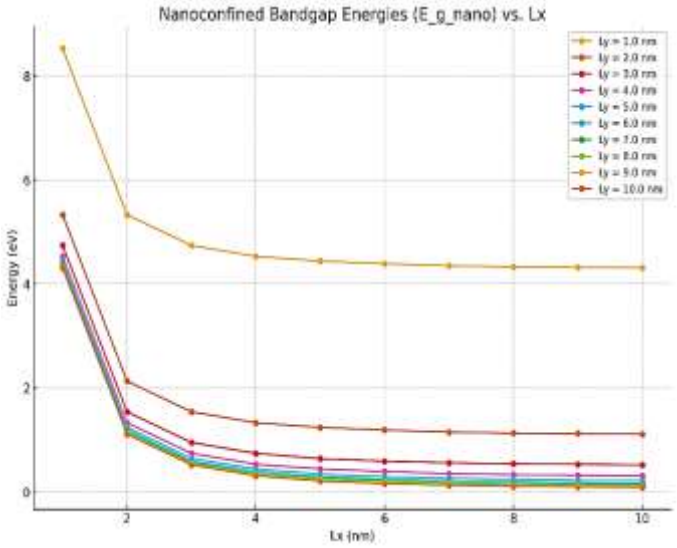

Figure 1: Nanoconfined Bandgap Energies $E_{g,nano}$ vs. L_x

The results presented in Table 1 and Figure 1 demonstrate a pronounced impact of quantum confinement on the bandgap energy of MoS_2. As the confinement dimensions (L_x and L_y) decrease, the bandgap energy increases, consistent with the enhanced quantum confinement effect. Figure 1 illustrates the relationship between nanoconfined bandgap energies ($E_{g,nano}$) and varying confinement dimensions (L_x) for fixed values of L_y . The plot reveals that for a given L_y , the bandgap energy decreases with increasing L_x , with a more pronounced effect at lower L_y values. For instance, at $L_y = 1nm$, the bandgap energy drops sharply from 5.02 eV at $L_x = 1nm$ to approximately 2.54 eV at $L_x = 10nm$. Similarly, for $L_y = 10nm$ he bandgap energy ranges from 2.54 eV to 0.05 eV as L_x increases from 1 nm to 10 nm.

Figure 2 shows the average nanoconfined bandgap energies as a function of L_y for different values of L_x . The trend is similar to that observed for varying L_x, where the bandgap energy decreases as $L_y$increases. This decrease in energy is indicative of the reduction in quantum confinement effects as the dimensions increase.

The optimal dimensions for photocatalytic water splitting, where the bandgap energy falls within the range suitable for water splitting (1.23 eV to 2.2 eV), can be identified from the table and the graphs. For example, with $L_x = 2$nm and $L_y = 2nm$, the bandgap energy is approximately 1.26 eV, making it a promising candidate for efficient photocatalytic water splitting.

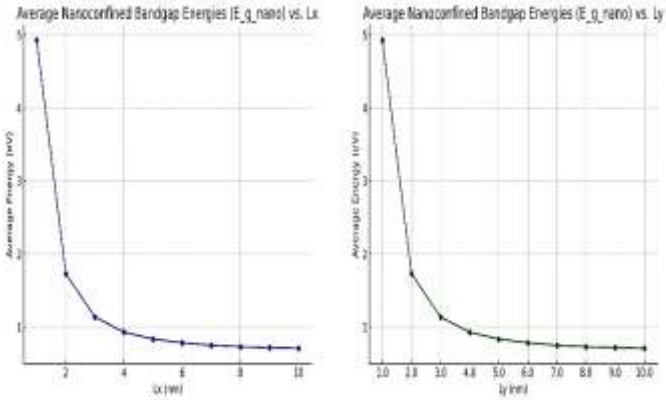

Figure 2: Average Nonconfined Bandgap Energies at varying L_x and L_y dimensions.

Table 2 shows the calculated energy levels and bandgap changes for a fixed confinement dimension of $L_y = 2nm$, with varying $L_x$dimensions ranging from 1 nm to 10 nm.

TABLE 2: Calculated Bandgap Energies Levels and Changes at $L_y = 2nm$

L_x(nm)	E_V(eV)	E_C(eV)	$E_{g,nano}$(eV)	ΔE_g(eV)
1.0	3.138	8.472	5.334	3.534
2.0	1.255	3.389	2.134	0.334
3.0	0.906	2.447	1.541	-0.259
4.0	0.784	2.118	1.334	-0.467
5.0	0.728	1.965	1.237	-0.563
6.0	0.697	1.883	1.185	-0.615
7.0	0.679	1.833	1.154	-0.646
8.0	0.667	1.800	1.133	-0.667
9.0	0.659	1.778	1.119	-0.681
10.0	0.653	1.762	1.109	-0.691

The results demonstrate a decrease in bandgap energy as L_x increases, aligning with the trend observed for varying L_y dimensions. This table enables the identification of optimal confinement dimensions for photocatalytic water splitting, where the bandgap energy falls within the desired range of $1.23\ eV\ to\ 2.2\ eV$. Specifically, a confinement dimension of $L_x = 2nm$ and $L_y = 2nm$ yields a bandgap energy of approximately 2.134 eV, making it suitable for photocatalytic application.

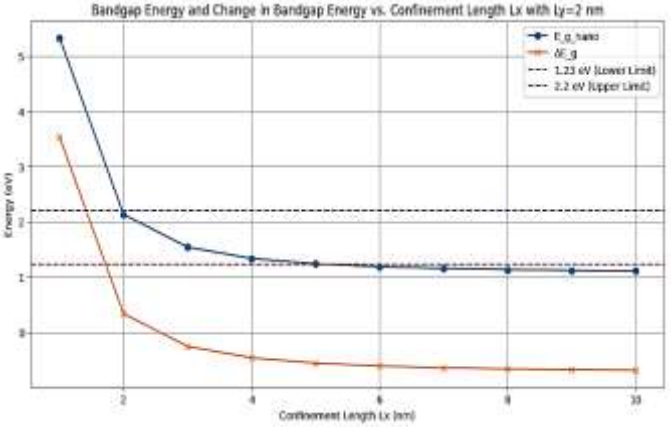

Figure 3(a): Variation of Bandgap Energy and Change in Bandgap Energy with dimensions of L_x

Moses G. Udoisoh, "Theoretical Investigation of Quantum Confinement Effects on Bandgap Changes in MoS_2 for Photocatalytic Water Splitting," *International Journal of Multidisciplinary Research and Publications (IJMRAP)*, Volume 7, Issue 2, pp. 132-136, 2024.

Figure 3 presents the bandgap energy $E_{g,nano}$ and its change (ΔE_g) as a function of confinement length L_x with L_y fixed at 2 nm.

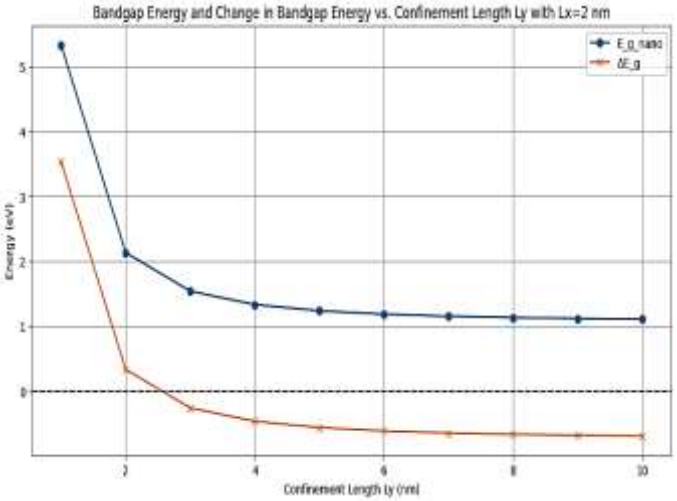

Figure 3(b): Variation of Bandgap Energy and Change in Bandgap Energy with dimensions of L_y with $L_x = 2$nm

The plot includes horizontal lines at 1.23 eV and 2.2 eV to indicate the optimal range for photocatalytic water splitting.

Table 3 provides the calculated energy levels and bandgap changes for equal confinement dimensions ($L_x = L_y = L$) ranging from 1 nm to 10 nm.

TABLE 3: Calculated Bandgap Energies and Changes at $L_x = L_y = L$

L(nm)	E_V(eV)	E_C(eV)	$E_{g,nano}$(eV)	ΔE_g(eV)
1	2.510	6.777	4.267	2.467
2	0.628	1.694	1.067	-0.733
3	0.279	0.753	0.474	-1.325
4	0.157	0.424	0.267	-1.533
5	0.100	0.271	0.171	-1.629
6	0.070	0.188	0.119	-1.681
7	0.051	0.138	0.087	-1.713
8	0.039	0.106	0.067	-1.733
9	0.031	0.084	0.053	-1.747
10	0.025	0.068	0.043	-1.757

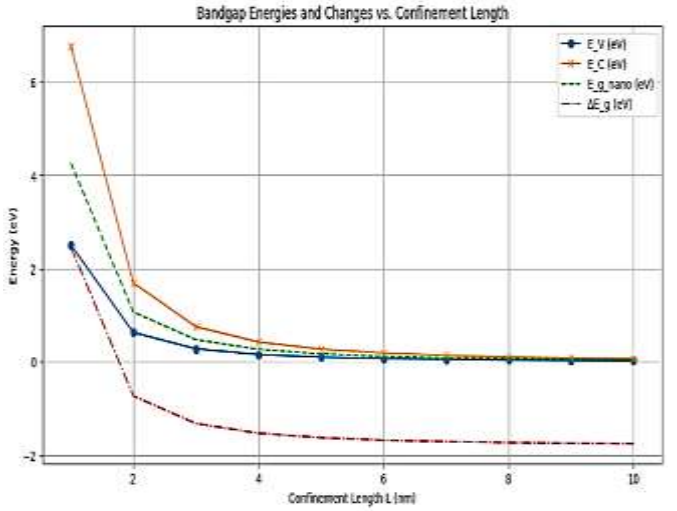

Figure 4: Variation of Bandgap Changes vs. Confinement Length $L_x = L_y = L$

The results show a similar trend where the bandgap energy decreases as the confinement dimensions increase. At $L = 1\ nm$, the bandgap energy is at its highest (4.267 eV), and it decreases significantly to 0.043 eV at $L = 10\ nm$.

Figure 4 presents the energy energies (E_V *and* E_C), the nano bandgap energy ($E_{g,nano}$), and the change in bandgap energy (ΔE_g) as functions of the confinement length L for equal confinement dimensions ($\boldsymbol{L_x = L_y = L}$).

This plot provides a comprehensive view of how these energy values vary with the confinement dimensions.

IV. Discussion

This study demonstrates that quantum confinement significantly impacts the bandgap energy of MoS_2, enabling tunability for optimized photocatalytic water splitting performance.

Nano Bandgap Energies for Varying Confinement Dimensions

The calculated nano bandgap energies reveal a substantial increase in bandgap energy as confinement dimensions decrease, consistent with the quantum confinement effect. For instance, the bandgap energy reaches a maximum value of 5.02 eV when both confinement dimensions are at their minimum (1 nm). Conversely, as the confinement dimensions increase to $10nm$, the bandgap energy decreases to approximately 0.05 eV. This trend highlights the tunability of the bandgap energy through precise control of the nanomaterial's dimensions, making it possible to tailor the material for specific applications.

Bandgap Energy and Changes for Fixed L_y = 2 nm

For a fixed L_y= 2 nm, the bandgap energy decreases as $L_x$increases, with a steep decrease at smaller L_x values that gradually flattens out as Lx approaches 10 nm. Notably, the optimal range for photocatalytic water splitting (1.23 eV to 2.2 eV) is achieved when L_x is approximately $2nm$, yielding a bandgap energy of 2.134 eV. This optimal range is crucial for efficient photocatalytic water splitting, as it allows for maximum absorption of visible light.

Energy Levels and Bandgap Changes for Equal Confinement Dimensions

When L_x and L_y are equal, the energy levels and the nano bandgap energy show a consistent decrease with increasing confinement length. At a confinement length of 1 nm, the bandgap energy is at its highest (4.267 eV), and it decreases significantly to 0.043 eV at a confinement length of 10 nm. This trend underscores the impact of quantum confinement in enhancing the bandgap energy at smaller dimensions.

Critical Discussion

The findings from this study underscore the importance of quantum confinement in tuning the electronic properties of MoS_2. While reducing dimensions enhances certain properties, it is essential to balance these changes to ensure the material remains suitable for its intended application, considering factors like visible light absorption and material stability. The very high bandgap energies observed at extremely small

Moses G. Udoisoh, "Theoretical Investigation of Quantum Confinement Effects on Bandgap Changes in MoS_2 for Photocatalytic Water Splitting," *International Journal of Multidisciplinary Research and Publications (IJMRAP)*, Volume 7, Issue 2, pp. 132-136, 2024.

dimensions (e.g., 5.02 eV at 1 nm) may limit the material's absorption of visible light, which is crucial for photocatalytic applications.

V. Conclusion

This study showcases the potential of quantum confinement in optimizing MoS_2 properties for photocatalytic water splitting, offering valuable insights for advanced photocatalyst design and development. By carefully selecting the confinement dimensions, it is possible to achieve bandgap energies within the optimal range for this application, thus enhancing the material's efficiency.

Limitations and Further Studies

While this study provides critical insights, it is based on theoretical calculations that assume ideal conditions. Real-world factors such as defects, impurities, and surface states can influence the observed properties and should be considered in future research. Additionally, experimental validation of these theoretical predictions is necessary to confirm the practical applicability of the findings. Future studies should explore the effects of different confinement geometries, such as quantum wells and quantum wires, on the bandgap energy of MoS_2. Investigating the impact of environmental factors, such as temperature and pressure, on the quantum confinement effects would also provide a more comprehensive understanding. Finally, integrating $MoS_2$with other materials to form heterostructures could offer new avenues for enhancing its photocatalytic performance.

References

[1]. Abe, R., Sayama, K., & Sugihara, H. (2005). Development of new photocatalytic water splitting into h2 and o2 using two different semiconductor photocatalysts and a shuttle redox mediator io3-/i-. The Journal of Physical Chemistry B, 109(33), 16052-16061. https://doi.org/10.1021/jp052848l

[2]. Aggarwal, T., Ganguly, S., & Saha, D. (2021). Carrier recovery from sub-bandgap states in a gan-based quantum-confined structure: identification of carrier reservoirs through femtosecond pump-probe spectroscopy. The Journal of Physical Chemistry C, 125(6), 3535-3541. https://doi.org/10.1021/acs.jpcc.0c09892

[3]. Aggarwal, T., Udai, A., Pendem, V., Ganguly, S., & Saha, D. (2020). Femto-second carrier and photon dynamics in site controlled hexagonal ingan/gan isolated quantum dots: natural radial potential well and its dynamic modulation. Acs Photonics, 7(9), 2555-2561. https://doi.org/10.1021/acsphotonics.0c00905

[4]. Almansoori, M. (2023). Enhanced uv absorption by 2d mos2 nanoparticles. Ecs Transactions, 111(2), 47-51. https://doi.org/10.1149/11102.0047ecst

[5]. Chang, K., Mei, Z., Wang, T., Kang, Q., Ouyang, S., & Ye, J. (2014). Mos2/graphene cocatalyst for efficient photocatalytic h2 evolution under visible light irradiation. Acs Nano, 8(7), 7078-7087. https://doi.org/10.1021/nn5019945

[6]. Cheng, Y. (2023). Novel high entropy alloy (agalcuniti) hybridized mos2/si nanowires heterostructure with plasmonic enhanced photocatalytic activity.. https://doi.org/10.1117/12.2676326

[7]. Cui, X., Yang, X., Xian, X., Tian, L., Tang, H., & Liu, Q. (2018). Insights into highly improved solar-driven photocatalytic oxygen evolution over integrated ag3po4/mos2 heterostructures. Frontiers in Chemistry, 6. https://doi.org/10.3389/fchem.2018.00123

[8]. Gough, J., O'Brien, M., McEvoy, N., Bell, A., Duesberg, G., & Bradley, A. (2017). Enhancing the electrical properties of mos<inf>2</inf> through nonradiative energy transfer.. https://doi.org/10.1109/metamaterials.2017.8107862

[9]. Gusarov, S. (2024). Advances in computational methods for modeling photocatalytic reactions: a review of recent developments. Materials, 17(9), 2119. https://doi.org/10.3390/ma17092119

[10]. Новоселов, К., Mishchenko, A., Carvalho, A., & Neto, A. (2016). 2d materials and van der waals heterostructures. Science, 353(6298). https://doi.org/10.1126/science.aac9439

[11]. Ito, R., Akatsuka, M., Ozawa, A., Kato, Y., Kawaguchi, Y., Yamamoto, M., … & Yoshida, T. (2019). Photocatalytic activity of ga2o3 supported on al2o3 for water splitting and co2 reduction. Acs Omega, 4(3), 5451-5458. https://doi.org/10.1021/acsomega.9b0004

[12]. Kang, J., Liu, W., Sarkar, D., Jena, D., & Banerjee, K. (2014). Computational study of metal contacts to monolayer transition-metal dichalcogenide semiconductors. Physical Review X, 4(3). https://doi.org/10.1103/physrevx.4.031005

[13]. Lin, Y., Wang, X., Fu, X., & Su, W. (2022). in situ growth of crystalline carbon nitride on laocl for photocatalytic overall water splitting. Journal of Materials Chemistry A, 10(15), 8252-8257. https://doi.org/10.1039/d2ta00068g

[14]. Nawz, T., Safdar, A., Hussain, M., Lee, D., & Siyar, M. (2020). Graphene to advanced mos2: a review of structure, synthesis, and optoelectronic device application. Crystals, 10(10), 902. https://doi.org/10.3390/cryst10100902

[15]. Rouzhahong, Y., Wushuer, M., Mamat, M., Wang, Q., & Wang, Q. (2020). First principles calculation for photocatalytic activity of gaas monolayer. Scientific Reports, 10(1). https://doi.org/10.1038/s41598-020-66575-9

[16]. Srinivasadesikan, V., Varadaraju, C., Raghunath, P., & Lee, S. (2022). Applications of density functional theory on heavy metal sensor and hydrogen evolution reaction (her).. https://doi.org/10.5772/intechopen.99825

[17]. Sun, Y. (2023). Strain-modulated band structure and high harmonic generations in two-dimensional mos2. Journal of Physics Conference Series, 2608(1), 012033. https://doi.org/10.1088/1742-6596/2608/1/012033

[18]. Wang, J., Cui, C., Kong, Q., Ren, C., Li, Z., Qu, L., … & Jiang, K. (2018). Mn-doped g-c3n4 nanoribbon for efficient visible-light photocatalytic water splitting coupling with methylene blue degradation. Acs Sustainable Chemistry & Engineering, 6(7), 8754-8761. https://doi.org/10.1021/acssuschemeng.8b01093

[19]. Wang, L., Wang, Z., Wang, H., Grinblat, G., Huang, Y., Wang, D., … & Sun, H. (2017). Slow cooling and efficient extraction of c-exciton hot carriers in mos2 monolayer. Nature Communications, 8(1). https://doi.org/10.1038/ncomms13906

[20]. Yin, Z., Chen, B., Bosman, M., Cao, X., Chen, J., Zheng, B., … & Zhang, H. (2014). Au nanoparticle-modified mos2 nanosheet-based photoelectrochemical cells for water splitting. Small, 10(17), 3537-3543. https://doi.org/10.1002/smll.201400124

[21]. Yuan, Z., Wu, P., & Chen, Y. (2021). Optical resonator enhanced photovoltaics and photocatalysis: fundamental and recent progress. Laser & Photonics Review, 16(2). https://doi.org/10.1002/lpor.202100202

[22]. Zhang, C., Liu, A., Li, K., Du, Y., & Yang, P. (2019). One-step synthesis of mos2/tisi2 via an in situ photo-assisted reduction method for enhanced photocatalytic h2 evolution under simulated sunlight illumination. Catalysts, 9(3), 299. https://doi.org/10.3390/catal9030299

[23]. Zhang, Y., Zhang, Y., Li, X., Dai, J., Song, F., Cao, X., … & Crittenden, J. (2019). Enhanced photocatalytic activity of sic-based ternary graphene materials: a dft study and the photocatalytic mechanism. Acs Omega, 4(23), 20142-20151. https://doi.org/10.1021/acsomega.9b01832